Reprinted from TEXTILE RESEARCH JOURNAL, Vol. 59, No. 5, May 1989
Printed in U. S. A.

Theory of the Compression Hysteresis of Fibrous Assemblies

GARTH A. CARNABY

Wool Research Organisation of New Zealand, Christchurch, New Zealand

N. PAN

China Textile University, Shanghai, People's Republic of China

ABSTRACT

An analysis of a fibrous assembly at large deformations has been explored as a means of predicting the compressional behavior, especially the compression hysteresis. The essential principle is to classify all the fiber contact points in the assembly as either slipping or nonslipping, so they can be dealt with separately. The compressional modulus and Poisson's ratio are derived and shown to be dominated by the mechanical properties and the directional distribution of the individual fibers within the assembly. An iterative algorithm, in which the system geometry is updated on successive increments, is developed to cope with large and nonlinear deformations. A comparison between the theoretical prediction and the experiment has indicated reasonable agreement. An improvement could probably be achieved by including the contribution of fiber viscoelasticity to the total hysteresis.

The mechanical behavior of a unit cell of fibrous material is a subject of fundamental importance in the science of textile assemblies [11]. The compression properties of such a unit cell have been studied quite extensively using various types of apparatus [4], but the theoretical explanation of the observed compression behavior of the assembly in terms of the combined behavior of the individual fibers comprising it has remained largely unsatisfactory.

For many years, this subject was dominated by an important early paper by van Wyk [12]. Some thirty years later, Komori and Makishima [7] identified and developed their concepts of analysis based on the orientation density distribution. Lee and Lee [9] have recently used these concepts to create a much more comprehensive mechanical analysis.

Both of the important theoretical mechanical studies [9, 12] postulated that the compressive strain of the assembly of fibers is translated directly into bending strains in the individual fibers, and that the resistance of the assembly to an externally imposed stress arises solely from the resulting increase in bending energy in the fibers. Other workers have also recognized [3, 4], however, that the compression of fibrous masses causes large and significant fiber-fiber slippage, much of which is irreversible.

The incorporation of this second mechanism by which the fibers can accommodate the change in dimensions of the assembly is the main novel feature of our current analysis. It has made possible the theoretical prediction of the full hysteresis curve for compression and recovery. As the response of the material is nonlinear, it is presented as a tangent compliance term dependent on the initial state of stress and strain [2]. As such, it is in a form suitable for incorporation into a nonlinear computational package such as a finite-element formulation, in which the materials property matrix must be specified by the user.

Definition of the System Geometry

The analysis of the assembly of fibers proceeds from a consideration of one section of length $2b$ of an arbitrarily chosen fiber whose direction with respect to the conventional coordinate system is defined by the polar angle θ and the azimuthal angle ϕ, where $0 \leqslant \theta \leqslant \pi$ and $0 \leqslant \phi \leqslant \pi$, as shown in Figure 1. This approach was pioneered by Lee and Lee [9], and we have kept to their notation as far as possible. Although our analysis was partly inspired by their work and starts in the same way, there are important differences, however, and we will point these out as the analysis develops and diverges.

Let us assume [9] that for the fiber assembly in question, the probability that a fiber lies in the infinitesimal range of θ to $\theta + d\theta$ and ϕ to $\phi + d\phi$ is given by $\Omega(\theta, \phi) \sin \theta d\theta d\phi$, where $\Omega(\theta, \phi) \sin \theta$ is the density function of orientation of the fibers. Komori and Makishima [7] showed that under these conditions,

$$b = V/2DLI \quad , \tag{1}$$

0040-5175/89/59005-275$2.00

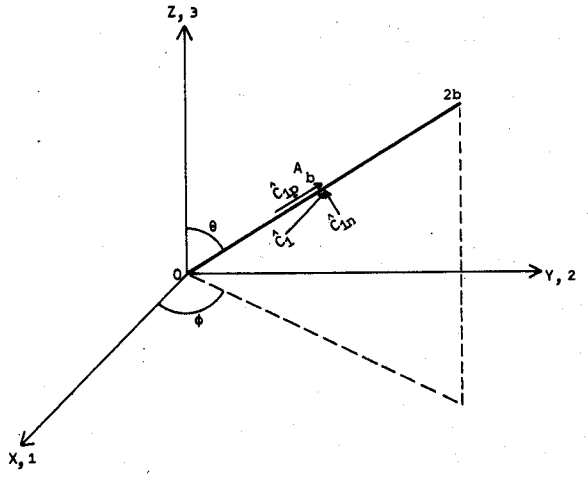

FIGURE 1. Definition of coordinate system, fiber orientation, and direction of forces.

$$n_v = DL^2I/V \quad , \tag{2}$$

$$I = \int_0^{\pi} d\theta \int_0^{\pi} d\phi J(\theta, \phi)\Omega(\theta, \phi) \sin\theta \quad , \tag{3}$$

$$J = \int_0^{\pi} d\theta' \int_0^{\pi} d\phi' \Omega(\theta', \phi') \sin\theta' [1 - \{\cos\theta \cos\theta' + \sin\theta \sin\theta' \cos(\phi - \phi')\}^2]^{1/2} \quad , \tag{4}$$

where b = mean free fiber length, D = fiber diameter, L = total length of fiber in volume V, V = volume of the fiber assembly, and n_v = number of contacts in volume V.

In Figure 1,

$$\overrightarrow{OA} = b(\sin\theta \cos\phi \hat{i}_1 + \sin\theta \sin\phi \hat{i}_2 + \cos\theta \hat{i}_3) \quad , \tag{5}$$

where $\hat{i}_1$, $\hat{i}_2$, and $\hat{i}_3$ are the unit vectors in the x, y, and z directions. Hence the mean projection of the section $\overrightarrow{OA}$ on the axes 1, 2, and 3 for the given direction density function is [9]

$$\bar{b}_j = \frac{2V}{DLI} K_j \quad j = 1, 2, 3 \quad , \tag{6}$$

where

$$K_1 = \int_0^{\pi/2} d\phi \int_0^{\pi/2} d\theta \sin^2\theta \cos\phi \, \Omega(\theta, \phi) \quad , \tag{7}$$

$$K_2 = \int_0^{\pi/2} d\phi \int_0^{\pi/2} d\theta \sin^2\theta \sin\phi \, \Omega(\theta, \phi) \quad , \tag{8}$$

and

$$K_3 = \int_0^{\pi/2} d\phi \int_0^{\pi/2} d\theta \sin\theta \cos\theta \, \Omega(\theta, \phi) \quad . \tag{9}$$

Mechanical Interaction Between Fibers

Consider at this stage the interaction between two fibers at one arbitrarily chosen point as shown in Figure 2. Grosberg [5] and Grosberg and Smith [6] showed that even in the absence of any external load applied to a mass of fibers, there were still significant nonzero contact forces between fibers in the assembly, since the fibers are prevented from recovering their lowest energy configuration because of mutual interference and frictional restraints to slippage.

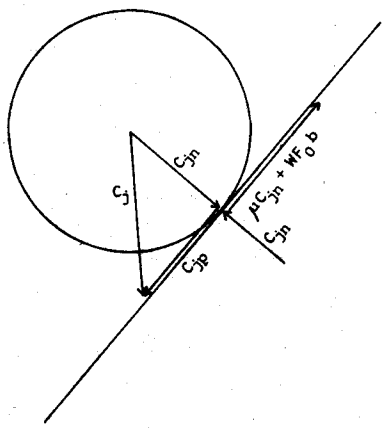

FIGURE 2. Interaction between two fibers at a contact point.

This interaction can be detected by single fiber withdrawal experiments. Grosberg and Smith [5, 6] have shown theoretically that the withdrawal force WF per unit length of fiber is approximately proportional to the external pressure P, but they also showed that when $P = 0$, a finite withdrawal force is needed. This arises because when P is reduced to zero, there is still a nonzero force at the contact points. One interpretation is that we might write

$$WF = \mu' P + WF_0 \quad , \tag{10}$$

where P = external pressure applied to the fiber mass, μ' = proportionality factor with dimensions of length, and WF_0 = value of WF when $P = 0$. This means that even in the absence of any external load on the fiber mass, the slippage of the top fiber in Figure 2 along the fiber in the direction of its axis would be opposed on average by a frictional force equal in value to $WF_0 b$.

Now consider that an external compressive load is applied to the assembly as a whole in the j direction such that the fiber contact point is required to sustain a contact force C_j as shown. This force C_j may be resolved into C_{jn} normal to the bottom contacting fiber

and C_{jp} parallel to it. The top fiber will thus begin to slide along the bottom fiber if

$$C_{jp} \geq C_{jn}\mu + WF_0 b \quad , \tag{11}$$

where μ = coefficient of friction between two contacting fibers. If the unit cell is subject to a combined compressive load (such as in a piston and cylinder device), the criterion for slippage given in Equation 11 remains the same, but the values used for C_{jn} and C_{jp} must also include the components of force due to pressure exerted in the other orthogonal directions. Let C_1, C_2, and C_3 be the net contact forces per contact in the 1, 2, and 3 directions as shown in Figure 1. Lee [8] showed that the components of C_j normal and parallel to the arbitrary fiber section shown in Figure 1 are

$$\begin{aligned} C_{1n} &= C_1(1 - \sin^2\theta\cos^2\phi)^{1/2} & C_{1p} &= C_1 \sin\theta\cos\phi \\ C_{2n} &= C_2(1 - \sin^2\theta\sin^2\phi)^{1/2} & C_{2p} &= C_2 \sin\theta\sin\phi \\ C_{3n} &= C_3 \sin\theta & C_{3p} &= C_3\cos\theta \quad . \end{aligned} \tag{12}$$

Equation 11 is thus equivalent for the general loading case to

$$\sum_i C_{jp} \geq \mu \sum_i C_{jn} + WF_0 b \quad , \tag{13}$$

that is,

$$\begin{aligned} &C_1 \sin\theta\cos\phi + C_2 \sin\theta\sin\phi + C_3\cos\theta \\ &\geq \mu\{C_1(1 - \sin^2\theta\cos^2\phi)^{1/2} \\ &+ C_2(1 - \sin^2\theta\sin^2\phi)^{1/2} \\ &\qquad + C_3 \sin\theta\} + WF_0 b \quad . \end{aligned} \tag{14}$$

We have as yet found no general analytical solution to Equation 14, although it is fundamental to the development of a general tangent compliance matrix. A solution for the special case of uniaxial compression is relatively straightforward, however, and we present it here because it still provides new insights into the classical problem of the compression of fibrous masses.

Effect of Slippage on Geometrical Parameters

If we now consider only the three separate possibilities for uniaxial compression of an arbitrarily oriented fibrous mass, then using Equation 12 we obtain from Equation 11 the following three equations:

for $C_1 \neq 0$, $C_2 = C_3 = 0$,

$$C_1 \sin\theta\cos\phi \geq C_1(1 - \sin^2\theta\cos^2\phi)^{1/2}\mu + WF_0 b \quad ; \tag{15a}$$

for $C_2 \neq 0$, $C_1 = C_3 = 0$,

$$C_2 \sin\theta\sin\phi \geq C_2(1 - \sin^2\theta\sin^2\phi)^{1/2}\mu + WF_0 b \quad ; \tag{15b}$$

for $C_3 \neq 0$, $C_1 = C_2 = 0$,

$$C_3\cos\theta \geq C_3 \sin\theta\,\mu + WF_0 b \quad . \tag{15c}$$

Equation 15c reveals that for compression in direction 3, there is a critical polar angle θ_c that dictates whether a contacting fiber will slip on the arbitrary fiber section shown in Figure 2. This critical angle is independent of the azimuthal angle. The equations for compression in the other two directions reveal a more complex criterion for slippage, though this is simply a consequence of the arbitrary choice of the orientation of the polar coordinate system. The geometrical parameters such as $\Omega(\theta, \phi)$ can equally well be expressed in terms of a different coordinate system where the polar and azimuthal angles are redefined to refer to different axes. Let us define three sets of polar coordinate systems as described in Table I and illustrated for compression in direction 1 in Figure 3. Using the angles as defined in Table I, we thus have three equations of identical form for the three load cases defined in Equation 15:

$$C_1\cos\alpha \geq C_1 \sin\alpha\,\mu + WF_0 b \quad , \tag{16a}$$

$$C_2\cos\psi \geq C_2 \sin\psi\,\mu + WF_0 b \quad , \tag{16b}$$

$$C_3\cos\theta \geq C_3 \sin\theta\,\mu + WF_0 b \quad . \tag{16c}$$

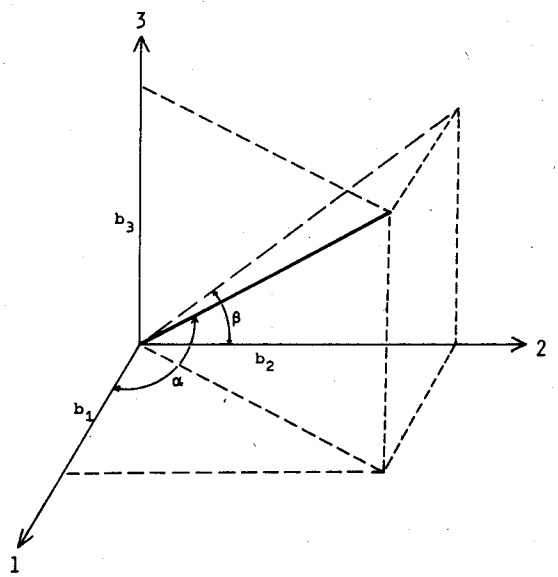

FIGURE 3. Redefinition of polar and azimuthal angles to define the slippage condition due to a net contact force in direction 1.

TABLE I. Polar coordinate systems used to determine the three critical angles in the three Cartesian directions.

j	Direction	Polar angle	Azimuthal angle
1	x	α	β
2	y	ψ	γ
3	z	θ	ϕ
j	j	χ_j	τ_j in general

In general this can be written as

$$C_j \cos \chi_j \geqslant C_j \sin \chi_j \mu + WF_0 b \quad . \tag{16}$$

We can find the critical value of χ_{cj} at which slippage begins for each of the three directions j by solving Equation 16 for the three cases of limiting friction:

$$\cos \chi_{cj} - \mu \sin \chi_{cj} = WF_0 b / C_j \quad , \tag{17}$$

whence

$$\sin \chi_{cj} = \frac{-\dfrac{\mu WF_0 b}{C_j} \pm \left\{\dfrac{\mu^2 WF_0^2 b^2}{C_j^2} - (1+\mu^2)\left(\dfrac{WF_0^2 b^2}{C_j^2} - 1\right)\right\}^{1/2}}{1+\mu^2} \quad . \tag{18}$$

This depends only on the as yet unspecified value of C_j, the net additional force in the direction j, which is supported by the contact point in question. All the other variables in Equation 18 may be regarded as known. Hence once χ_{cj} is known, it follows that for $\chi_j \geqslant \chi_{cj}$ there is no slippage, and for $\chi_j < \chi_{cj}$ all points of contact on the fibers (or fiber sections) whose orientation are defined by χ_j will slip.

Accordingly it is necessary to define an effective mean free length between nonslipping contact points, the value of which depends on the direction j of the applied force. The value of this effective mean free length will ultimately determine the deformation of the assembly as a "system of bending units." At this stage, let us simply define the three values for b_j' (using the notation of Lee and Lee [9]):

$$b_j' = V/2DLI_j \quad , \tag{19}$$

where

$$I_j = 4 \int_{\chi_{cj}}^{\pi/2} d\chi_j \int_0^{\pi/2} d\tau_j J_j(\chi_j, \tau_j) \Omega(\chi_j, \tau_j) \sin \chi_j \quad , \tag{20}$$

and

$$J_j = 4 \int_{\chi_{cj}'}^{\pi/2} d\chi_j' \int_0^{\pi/2} d\tau_j' \Omega(\chi_j', \tau_j') \times \sin \chi_j' [1 - \{\cos \chi_j \cos \chi_j' + \sin \chi_j \times \sin \chi_j' \cos (\tau_j - \tau_j')^2\}]^{1/2} \quad . \tag{21}$$

The mean values of the projections of b_j' in the three directions are

$$\bar{b}_{jj}' = (2V/DLI_j) K_j \quad , \tag{22}$$

where K_j remains the same as given in Equations 7–9. Hence the effective number of contact points per unit volume n_{vj}' as viewed from the three directions becomes

$$n_{vj}' = DL^2 I_j / V \quad , \tag{23}$$

where those that slip have been eliminated in the calculation of I_j.

Note here that we will use an incremental method later to solve the equations for equilibrium for the unit fiber cell for large deformations. It will therefore be necessary to recalculate many of the geometrical parameters on the completion of each increment. This applies to the orientation distribution function, the volume V, and the value of C_j. The equations for doing this are given in the Appendix without derivation.

Net Force per Contact Point

The external stress on the unit fibrous cell must be transferred internally through the various contact points. Any given cross section normal to j will intersect stress-carrying sections of fibers but few if any actual contact points. Now following Lee and Lee [9], consider all the slipping and nonslipping contact points $n_{\bar{b}j}$ in a small volume $\bar{b}_j$ of unit cross-sectional area normal to j and of height $\bar{b}_j$. If SN is the proportion of contact points that slip, then the external stress P_j must be as follows:

$$P_j = SN n_{\bar{b}j} C_{sj} + (1 - SN) n_{\bar{b}j} C_j \quad , \tag{24}$$

where C_{sj} = mean value of the resistance per slipping contact point within $\bar{b}$, and C_j = average force per nonslipping contact point.

Now, from Lee and Lee [9]

$$n_{\bar{b}j} = 2LK_j / V \quad , \tag{25}$$

$$SN = 4 \int_0^{\chi_{cj}} \int_0^{\pi/2} \dot{\Omega}(\chi_j, \tau_j) \sin \chi_j d\chi_j d\tau_j \quad . \tag{26}$$

We can find the value of C_{sj} using Equation 16:

$$C_{sj} = 4 \int_0^{\chi_{cj}} d\chi_j \int_0^{\pi/2} d\tau_j \frac{\Omega(\chi_j, \tau_j) \sin \chi_j WF_0 b}{\cos \chi_j - \mu \sin \chi_j} \quad . \tag{27}$$

Since all the nonslipping contact points may be thought of as carrying an equal load,

$$C_j = \frac{(P_j - SNn_{bj}C_{sj})}{(1 - SN)n_{bj}} \quad . \tag{28}$$

Mechanism of Deformation

Both van Wyk [12] and Lee and Lee [9] made various simplifying assumptions before calculating the deflection of the fibers due to the action of the contact point forces. With reference to Figures 1 and 4 (from Lee and Lee [9]), we will consider a single, initially straight section of one fiber that is bounded by two nonslipping contact points at a distance $2b_j'$ apart. Let a third nonslipping contact point fall at the midpoint. If we consider a reference frame in which points A and C are fixed, we are interested in the deflection of the midpoint of the fiber section under the action of the midpoint contact force.

Let us assume that the fibers are all uniform, identical, and linearly elastic in bending. Torsion, compression, and extension of the fiber section are all considered negligible. No new contact points are formed for a small load or for an incremental increase in the load.

In his original paper, van Wyk [12] suggested that the correct beam deflection theory to use when calculating the deflection of point B is that for a beam with built-in ends. This equation ensures continuity in curvature at the contact points, conservation of mass, and no slippage at the contact points. Lee and Lee [9], however, used the equation for a beam with free ends, which we regard as inappropriate. We use van Wyk's equation [12] here, which results in a lower deflection by a factor of 4:

$$\delta_{jk} = \pm \frac{1}{6} \frac{C_j b_j'^3}{B} m_{jk} \quad (+, j \neq k; -, j = k) \quad , \tag{29}$$

where δ_{jk} = the mean deflection of the midpoint of all the fiber sections in direction k, B = the flexural rigidity of the fiber, and m_{jk} is as given by Lee and Lee [9]:

$$m_{11} = \int_0^{\pi/2} d\phi \int_0^{\pi/2} d\theta \times (1 - \sin^2\theta \cos^2\theta)\Omega(\theta, \phi) \sin\theta$$

$$m_{22} = \int_0^{\pi/2} d\phi \int_0^{\pi/2} d\theta \times (1 - \sin^2\theta \sin^2\phi)\Omega(\theta, \phi) \sin\theta$$

$$m_{33} = \int_0^{\pi/2} d\phi \int_0^{\pi/2} d\theta (\sin^2\theta)\Omega(\theta, \phi) \sin\theta$$

$$m_{12} = m_{21} = \int_0^{\pi/2} d\phi \int_0^{\pi/2} d\theta \times \sin^2\theta \sin\phi \cos\phi\, \Omega(\theta, \phi) \sin\theta$$

$$m_{23} = m_{32} = \int_0^{\pi/2} d\phi \int_0^{\pi/2} d\theta \times \sin\theta \cos\theta \sin\phi\, \Omega(\theta, \phi) \sin\theta$$

$$m_{31} = m_{13} = \int_0^{\pi/2} d\phi \int_0^{\pi/2} d\theta \times \sin\theta \cos\theta \cos\phi\, \Omega(\theta, \phi) \sin\theta \quad . \tag{30}$$

Equation 29 applies only for small strains of the bending element. In the incremental approach used to accommodate the large deformations of the assembly as a whole, we have assumed that the actual bending strains in the fibers remain small (the validity of this assumption depends on the geometry and particularly the distance between contact points). The incremental form of this equation as used here is

$$\Delta\delta_{jk} = \pm \frac{1}{6} \frac{\Delta C_j b_j'^3}{B} m_{jk} \quad . \tag{31}$$

Strictly speaking the case we present in this paper is also complicated by the possible action of additional slipping contact points acting on the fiber section shown in Figure 4 between points A and C. Their effect on the deflection of B is not likely to be large in most cases, however, because the contact force that can be sustained is generally small. Let us make the simplifying assumption that they have no net effect on the deflection of point B, and indeed that the slippage at these slipping contact points continues until the movement is such that the deflection of point B can be accommodated as dictated by Equation 31.

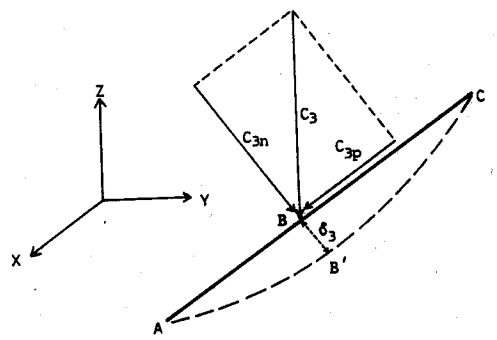

FIGURE 4. Deformation of a fiber element due to a contact point load C_3 (from Lee and Lee [9]).

Both van Wyk [12] and Lee and Lee [9] related the deflection of the midpoint of such a bending element

to the general compression of a layer of such bending units of thickness $\bar{b}_{jj}'$. In effect, they considered that such a layer would on average change in thickness by an amount equal to δ_{jj}. This seems the simplest assumption to make. Hence, proceeding on this basis for our uniaxial load cases, we have

$$\Delta\epsilon_j = \Delta\delta_{jj}/b_{jj}' \quad . \tag{32}$$

Stress-Strain Relationship

The general tangent compliance matrix for the unit fibrous cell may be written [2] as

$$\begin{Bmatrix} \Delta\epsilon_1 \\ \Delta\epsilon_2 \\ \Delta\epsilon_3 \\ \Delta\gamma_{12} \\ \Delta\gamma_{23} \\ \Delta\gamma_{31} \end{Bmatrix} = \begin{bmatrix} C_{T11} & C_{T12} & C_{T13} & C_{T14} & C_{T15} & C_{T16} \\ C_{T21} & C_{T22} & C_{T23} & C_{T24} & C_{T25} & C_{T26} \\ C_{T31} & C_{T32} & C_{T33} & C_{T34} & C_{T35} & C_{T36} \\ C_{T41} & C_{T42} & C_{T43} & C_{T44} & C_{T45} & C_{T46} \\ C_{T51} & C_{T52} & C_{T53} & C_{T54} & C_{T55} & C_{T56} \\ C_{T61} & C_{T62} & C_{T63} & C_{T64} & C_{T65} & C_{T66} \end{bmatrix} \times \begin{Bmatrix} \Delta\sigma_1 \\ \Delta\sigma_2 \\ \Delta\sigma_3 \\ \Delta\tau_{12} \\ \Delta\tau_{23} \\ \Delta\tau_{31} \end{Bmatrix} \quad , \tag{33}$$

which may be summarized as

$$\Delta\epsilon = [C_T(\sigma_0, \epsilon_0)]\Delta\sigma \quad . \tag{34}$$

In a previous paper coauthored by one of us, the value of the C_{T33} term in this matrix was explored for the special case of a transversely symmetric, oriented fiber bundle for large tensile strains in direction 3 of preferential orientation.

If we retain generality here regarding the orientation of the fibers, we must consider all twenty-one independent terms in the compliance matrix for the case of general anisotropy. In this paper, however, we are concerned only with the range in values of $\Delta\sigma$, which encompasses compressive stresses.

As we have not yet solved Equation 14 for the general combined compressive load case, we are concerned here with a valid solution only for the simple situations of compression where no more than one of the σ_{10}, σ_{20}, or σ_{30} terms is nonzero. In this case Equation 32 is applicable:

$$1/C_{Tjj} = E_{Tjj} = (-\Delta P_j/A_j)/\Delta\epsilon_j \quad , \tag{35}$$

and

$$-E_{Tjj}C_{Tjk} = \nu_{Tjk} = -\frac{\Delta\delta_{jk}/\bar{b}_{kk}'}{\Delta\delta_{jj}/\bar{b}_{jj}'} \quad , \tag{36}$$

where A_j is the cross-sectional area of the fiber assembly with respect to P_j; in the case of unit area, $A_j = 1$.

Substituting in Equation 35, using Equations 19, 22, 23, 25, 31, and 32, and using

$$B = E_f I_f \quad , \tag{37}$$

$$= E_f \eta \pi D^4/64 \quad , \tag{38}$$

where E_f = the fiber Young's modulus, I_f = the fiber moment of inertia, η = the shape factor of the fiber related to bending, and $V_f = \pi D^2 L/4V$ = the volume fraction of the assembly (39), we obtain

$$1/C_{Tjj} = E_{Tjj} = \frac{192}{\pi^2} E_f \eta V_f^3 \frac{K_j^2 I_j^2}{m_{jj}} \times \left(1 - SN + SN\frac{\Delta C_{sj}}{\Delta C_j}\right) \quad . \tag{40}$$

$$j = 1, 2, 3$$

Substituting in Equation 36, using Equations 22 and 31,

$$-E_{Tjj}C_{Tjk} = \nu_{Tjk} = \frac{m_{jk}K_j I_k}{m_{jj}K_k I_j} \quad \begin{matrix} j \neq k \\ j = 1, 2, 3 \\ k = 1, 2, 3 \end{matrix} \quad . \tag{41}$$

Incremental Geometry Changes and Fibrous Assembly Hysteresis

Because we will use an incremental method to cope with the large deformations typical of fibrous assemblies, it is necessary to define the algorithms that are to be used to update the system geometry on successive increments. Equations 40 and 41 show that the tangent compliance in compression C_{Tjj} and the Poisson's ratio ν_{jk} depend on various parameters that need to be updated: A_j, V_f, K_j, I_j, m_{jj}, K_k, m_{jk}, and I_k. Because the transverse stress remains zero, $I_k = I$ and this value also needs updating as the orientations change.

Let us consider the various stages in the classical case of a fibrous assembly with an initially random orientation of the fibers. In this case [7, 9, 12],

$$\Omega(\chi_j, \tau_j) \sin\chi_j = \sin\chi_j/2\pi \quad . \tag{42}$$

The fiber properties D, μ, WF_0, V_{f0}, E_f, η, and L are regarded as being known.

COMPRESSION STAGE

Calculation proceeds by the successive application of incremental loadings. In practice, a small arbitrary increase ΔC_j in the average force per nonslipping contact point C_j is applied. For each value of C_j, a corresponding critical angle χ_{cj} can be obtained from Equation 18. The mean resistance provided by each slipping contact point, C_{sj}, is then obtained through Equation 27. This gives us a value for ΔC_{sj}.

After calculating the relevant geometrical parameters I_j, I_k, K_j, K_k, m_{jk}, n_{bjj}, and m_{jj}, the value of P_j and hence ΔP_j follows from Equation 24. The values of $\Delta\epsilon_j$, E_{Tjj}, and ν_{Tjk} then follow from Equations 32, 40, and 41.

Before starting the next iteration, we must use the values of $\Delta\epsilon_j$ and ν_{Tjk} to update the geometry. The procedures are described in the Appendix.

RECOVERY STAGE

The external load is removed during this stage. In practice this is once again achieved by a succession of small decreases in the value of C_j, but the behavior of the slipping contact points is subtly different during recovery. Referring again to Figure 2, we see that now the cause of the recovery is the stored bending energy in the lower fiber, but this applies only a normal force to the slipping fiber. Even when the value of the normal force C_{jn} is reduced to zero, the top fiber will not slip back "up" the lower fiber.

We have considered two alternative assumptions to model the necessary return slippage in sympathy with the recovery of the bent fibers. The first option is to assume that if $C_{ij} < 0$, the contact will in fact be lost altogether, and hence the slipping contact points will contribute nothing during the recovery phase and will simply slip freely while carrying none of the reduced external load. The second option is to assume that a finite value of C_{ij} pointing in the reverse direction (up the lower fiber in Figure 2) is needed to overcome the resistance WF_0b at the contact. Under these conditions,

$$C_j \cos\theta = WF_0b \quad . \tag{43}$$

We prefer the second of these two options.

Hence the analysis proceeds in a fashion similar to that used previously, except that now

$$\Delta P_j = (1 - SN)n_{bj}\Delta C_j - SNn_{bj}\Delta C_{sj} \quad . \tag{44}$$

However, now

$$C_{sj} = 4\int_0^{\chi_{cj}} d\chi_j \int_0^{\pi/2} d\tau_j \Omega(\chi_j, \tau_j) \times \sin\chi_j WF_0b \sec\chi_j \quad . \tag{45}$$

The critical angle follows as before from Equation 18. The tangent modulus now becomes

$$E_{Tjj} = \frac{192}{\pi^2} E_f \eta V_f^3 \frac{K_j^2 I_j^2}{m_{jj}} \left(1 - SN - SN\frac{\Delta C_{sj}}{\Delta C_j}\right) \quad . \tag{46}$$

As recovery proceeds with reductions in C_j, the critical angle also reduces, but the changing orientation function also ensures more fibers at a lower polar angle. The path on recovery thus differs from the compression curve, and the external load P_j is reduced to zero, while the assembly still contains some strain energy in the bent fibers. This energy is now locked into the assembly by virtue of its own internal friction.

If the assembly is once again compressed, the stress-strain curve follows a new path different from the original path. The mechanism described in this paper thus provides a quantitative mechanical explanation for the well known compression hysteresis cycle of fibrous materials together with the continual reduction in resistance to compression on successive compression cycles.

Evaluation of the Theory

In order to evaluate the theoretical model, we conducted a number of unidirectional compression experiments using an Instron tensile tester with approximately random fiber assemblies. All the wool samples were prepared with identical volumes but different masses, *i.e.*, different volume fractions. The fiber properties needed are shown in Table II.

Figure 5 shows a comparison of the theoretical and experimental results for compression hysteresis. The

TABLE II. Fiber properties.

Property	Symbol	Value	Unit	Source
Mean fiber diameter	D	37	μm	measured
Fiber initial modulus	E_f	6.3×10^5	N/cm^2	[10]
Fiber shape factor for bending	η	1	-	assumed
Withdrawal force without loading	WF_0	0.17	mN/cm	[1]
Coefficient of friction between fibers	μ	0.3	-	[10]

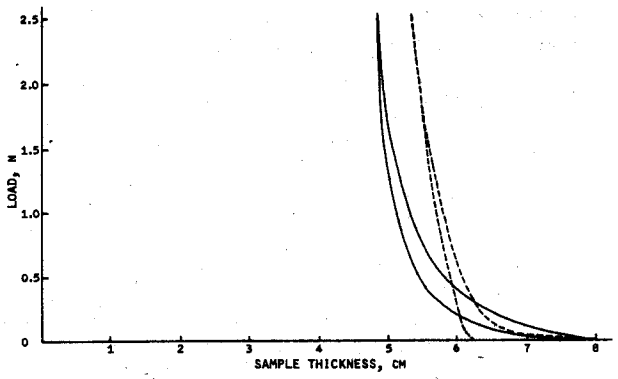

FIGURE 5. Comparison of theoretical (- - -) and experimental (——) results. $V_f = 0.00649$.

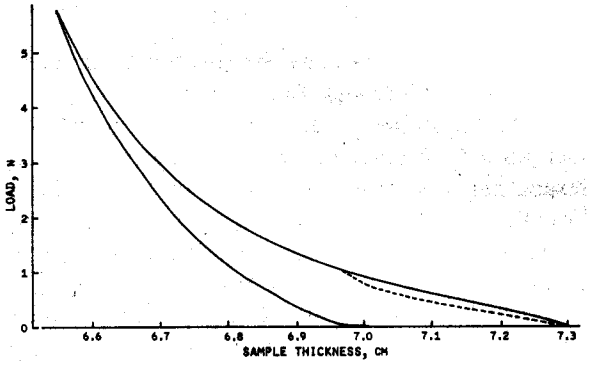

FIGURE 7. Mechanical behavior under large (——) and small (- - -) ranges of load. $V_{f0} = 0.1$.

full height of the test specimen is shown on the abscissa to indicate the scale of the inaccuracies. The predicted deformation is slightly smaller than that obtained experimentally, which indicates that the average modulus predicted is higher than the observed value. The width of the predicted hysteresis curve is somewhat narrower than the experimental curve, but this is to be expected because the viscoelastic nature of the fibers has been ignored. Figure 6 shows the predicted curves corresponding to repeated compression cycling.

with the results of Lee and Lee [9] for the initial compression stage as shown in Figure 8. Lee and Lee excluded the slippage mechanism from their analysis and, as they realized, this resulted in remarkably high values for the predicted initial modulus. Furthermore, Lee and Lee used the beam bending equation for free ends, which assumes four times greater flexibility than we have assumed here (and van Wyk [12] as well). In our model, however, the results are more consistent with the measured values.

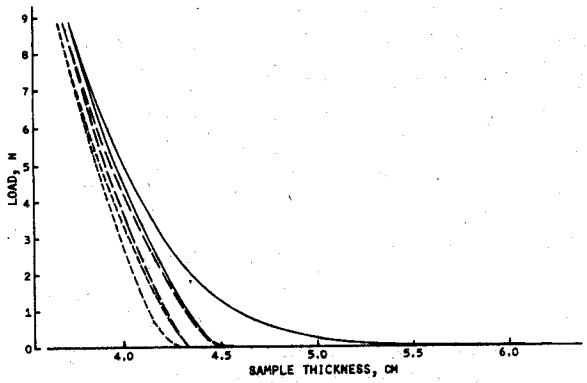

FIGURE 6. The mechanical response of a fiber assembly under repeated compression cycles. $V_{f0} = 0.0143$.

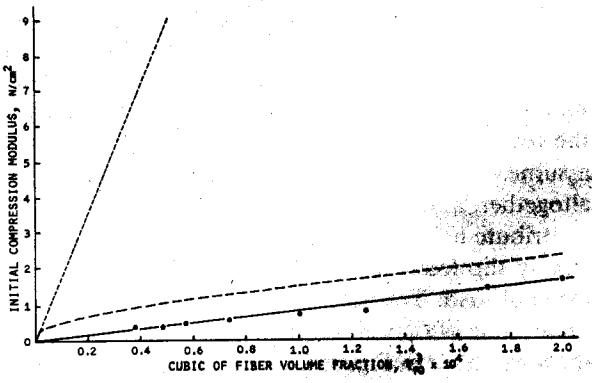

FIGURE 8. Initial compression modulus from different methods: (-----) predicted by Lee and Lee [9], (●——●) measured by Lee and Lee [9], (- - -) our prediction.

The predicted curves giving the response of a fiber assembly under small and large load ranges are shown in Figure 7. As the maximum load increases, the residual strain and the width of the hysteresis loop become larger. We predicted an almost linear elastic response for the small load case.

The effect of fiber slippage during compression can also be evaluated by comparing this theoretical model

Figure 9 shows the changes in Poisson's ratio in the compression stage. An interesting observation is that at some points, the values of Poisson's ratio are larger than 0.5, indicating the difference between a fiber assembly and an ordinary solid.

Table III gives some more detailed computer output data showing how various theoretical parameters alter during one compression and recovery cycle.

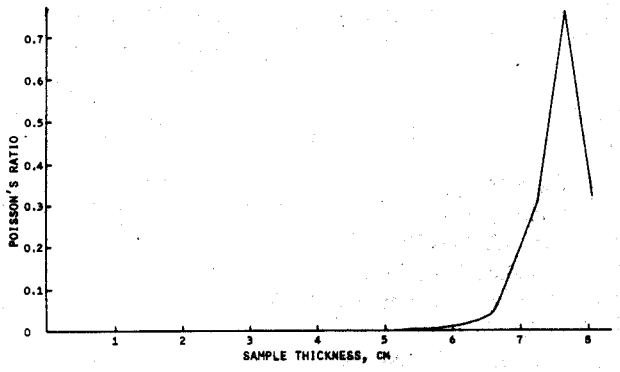

FIGURE 9. Changes in Poisson's ratio under compression and recovery. $V_{f0} = 0.00649$.

Conclusions

Under deformation, all the fiber contact points in a fibrous assembly can be divided into two categories of contact points according to whether they slip or do not slip, based on the criterion of the critical slipping angle. The different contributions of these two categories of fibers can then be treated separately so as to derive the modulus, Poisson's ratio, and other mechanical property parameters that are more realistic than previous results. Based on such a treatment, it is then possible to predict the mechanical behavior of fibrous assemblies under large deformations using an iteration technique. For each step of the iteration, as the load and the critical slipping angle increase, all such parameters

TABLE III. The changes in relevant parameters at each iteration step.[a]

T, cm	P_j, mN	X_{cj}, deg	V_{jk}	E_g, mN/cm²	E_s, mN/cm²	C_{sj}, mN/point	C_j, mN/point	SN	I_j
During compression									
8.05	9.0	10.574	0.3248	183.25	0.052	0.001	0.04	0.017	0.770
7.65	18.8	56.067	0.7606	19.26	3.636	0.029	0.12	0.434	0.327
7.25	29.8	66.006	0.3155	18.84	2.920	0.050	0.28	0.465	0.596
6.83	60.2	69.380	0.1332	61.98	3.493	0.050	0.52	0.368	1.003
6.59	111.5	70.875	0.0450	200.77	2.957	0.038	0.84	0.245	1.453
6.40	187.4	71.658	0.0283	391.94	2.590	0.033	1.25	0.199	1.637
6.24	287.1	72.116	0.0201	640.34	2.176	0.029	1.73	0.168	1.762
6.11	412.5	72.407	0.0155	939.5	1.814	0.025	2.29	0.146	1.852
5.99	569.5	72.603	0.0128	1303.3	1.474	0.023	2.92	0.124	1.922
5.88	755.0	72.741	0.0104	1733.2	1.245	0.021	3.64	0.111	1.979
5.79	974.0	72.842	0.0087	2223.6	1.060	0.019	4.44	0.100	2.024
5.72	1137.5	72.918	0.0069	2393.5	0.782	0.018	5.32	0.090	2.065
5.64	1355.4	72.976	0.0057	2652.0	0.642	0.017	6.29	0.085	2.090
5.56	1596.5	73.022	0.0048	2996.0	0.528	0.016	7.33	0.078	2.118
5.48	1858.0	73.059	0.0040	3375.3	0.437	0.014	8.44	0.072	2.144
5.40	2139.3	73.089	0.0035	3770.1	0.365	0.013	9.65	0.066	2.168
5.39	2191.1	73.093	0.0030	4185.7	0.340	0.012	9.81	0.062	2.189
5.38	2230.7	73.096	0.0029	4254.4	0.331	0.012	10.00	0.061	2.192
5.37	2272.8	73.100	0.0029	4308.4	0.324	0.012	10.17	0.060	2.195
5.36	2317.4	73.104	0.0028	4364.7	0.316	0.012	10.35	0.060	2.197
During recovery									
5.50	1692.6	73.104	0.0028	4424.2	0.123	0.005	7.55	0.059	2.200
5.64	1182.5	73.031	0.0036	3725.9	0.181	0.005	5.33	0.067	2.166
5.77	755.9	72.919	0.0045	3114.8	0.275	0.006	3.46	0.075	2.129
5.91	399.6	72.711	0.0059	2602.2	0.444	0.007	1.85	0.084	2.089
6.05	69.7	72.202	0.0082	2409.3	0.912	0.007	0.31	0.092	2.051
6.18	34.3	66.757	0.0096	2061.8	2.383	0.005	0.16	0.072	2.095
6.20	15.7	60.314	0.0096	2177.9	1.960	0.003	0.07	0.049	2.158
6.21	5.5	43.256	0.0093	2388.0	0.510	0.001	0.02	0.183	2.240
6.213	0.12	0	0.0092	2503.2	0	0	0	0	2.280
6.215	0.04	0	0.0092	2493.3	0	0	0	0	2.280
6.215	0.01	0	0.0092	2493.2	0	0	0	0	2.280
6.215	0	0	0.0092	2493.1	0	0	0	0	2.280

[a] T = sample thickness; $E_g + E_s = E_{ijj}$, where E_g and E_s are the contributions of nonslipping and slipping contact points, respectively; $j = 3$; $k = 1, 2$; cycle = 1; $V_{f0} = 0.00649$.

as the volume fraction and the directional distribution function have to be updated using the new critical slipping angle and the previous strain. The opposing effects of slipping fibers and unsymmetric parameter values in the compression and recovery stages are the main causes leading to different mechanical responses or mechanical hysteresis.

ACKNOWLEDGMENTS

We wish to acknowledge helpful discussions in the early stages of this project with various colleagues, notably Professors D. H. Lee and J. K. Lee, Drs. A. J. Carr and P. J. Moss, and Mr. A. M. Ford. Pan Ning wishes to thank the New Zealand Wool Board for providing financial support for his secondment to WRONZ so that this work could be done.

Appendix

We used the following equations to update the volume fraction and the orientation distribution function:

$$V_f = V_{f0}/(1 + 2\nu_{31}\epsilon_3 - \epsilon_3) \quad .$$

For the first step after starting from a random distribution,

$$\Omega(\chi_j', \tau_j) \sin \chi_j' d\chi_j' d\tau_j = \Omega(\chi_j, \tau_j) \sin \chi_j d\chi_j d\tau_j$$

$$= \frac{1}{2\pi}\left(\frac{H_1^2 \tan^2 \chi_j'}{1 + H_1^2 \tan^2 \chi_j'}\right)^{1/2} \times \frac{H_1 \sec^2 \chi_j'}{1 + H_1^2 \tan^2 \chi_j'} d\chi_j' d\tau_j \quad ,$$

and so on for subsequent increments when

$$H_1 = (1 + \epsilon_3)/(1 + \nu_{31}\epsilon_3) \quad .$$

The other parameters needing updating are all related to the orientation density distribution and may be recalculated once $\Omega(\chi_j', \tau_j)$ is known. These parameters include K_j, K_k, I_j, I_k, A_j, m_{jk}, n_{bj}, and m_{jj}.

Literature Cited

1. Carnaby, G. A., and Curiskis, J. I., The Tangent Compliance of Staple-fibre Bundles in Tension, *J. Textile Inst.* **78**, 293–305 (1987).
2. Curiskis, J. I., and Carnaby, G. A., Continuum Mechanics of the Fiber Bundle, *Textile Res. J.* **55**, 334–344 (1985).
3. Dunlop, J. I., On the Compression Characteristics of Fibre Masses, *J. Textile Inst.* **74**, 92–97 (1983).
4. Dunlop, J. I., Carnaby, G. A., and Ross, D. A., Bulk, I: The Bulk of Loose Wool, WRONZ Communication no. 28, 1974.
5. Grosberg, P., The Strength of Twistless Slivers, *J. Textile Inst.* **54**, T223–T233 (1963).
6. Grosberg, P., and Smith, P. A., The Strength of Slivers of Relatively Low Twist, *J. Textile Inst.* **57**, T15–T23 (1966).
7. Komori, T., and Makishima, K., Numbers of Fiber-to-fiber Contacts in General Fiber Assemblies, *Textile Res. J.* **47**, 13–17 (1977).
8. Lee, D. H., Initial Compressional Behaviour of Fibre Assembly (in Korean), Doctoral thesis, Seoul National University, 1985.
9. Lee, D. H., and Lee, J. K., Initial Compressional Behaviour of Fibre Assembly, in "Objective Measurement: Applications to Product Design and Process Control," S. Kawabata, R. Postle, and M. Niwa, Eds., The Textile Machinery Society of Japan, Osaka, 1985, pp. 613–622.
10. Morton, W. E., and Hearle, J. W. S., "Physical Properties of Textile Fibres," Butterworth, London, 1962.
11. Postle, R., Carnaby, G. A., and de Jong, S., "The Mechanics of Wool Fibre Assemblies," ch. 7, Ellis Horwood, Chichester, 1988.
12. van Wyk, C. M., Note on the Compressibility of Wool, *J. Textile Inst.* **37**, T285–T292 (1946).

Manuscript received March 9, 1988; accepted May 25, 1988.